

Supplementary Information

DMRT1-mediated reprogramming drives development of cancer resembling human germ cell tumors with features of totipotency

Taguchi et al.

Inventory of Supplementary Information

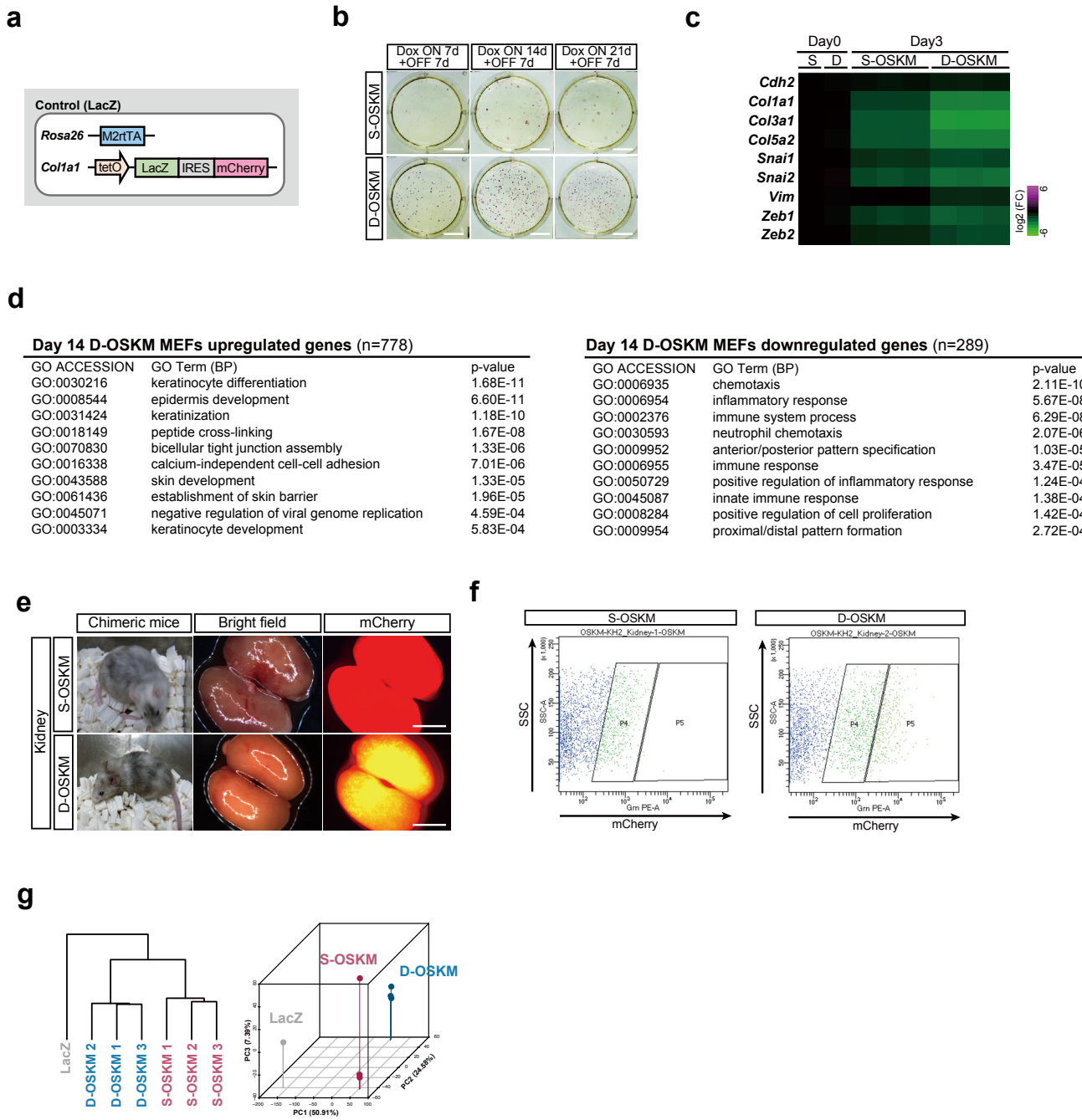
Supplementary Figures (Supplementary Figures 1-10)

Legends to Supplementary Figures

Reference

Supplementary Table S1

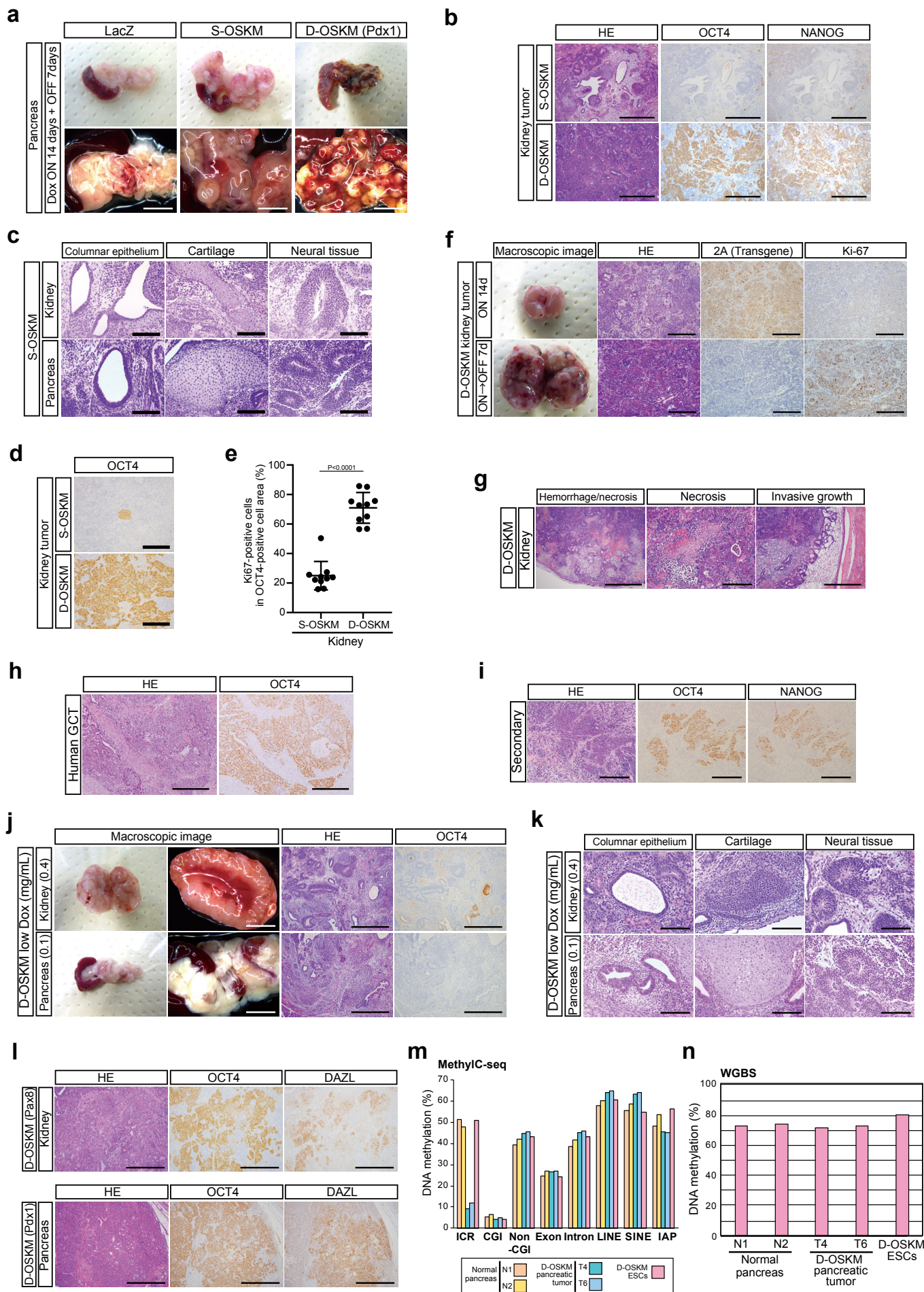
Supplementary Figure 1



Supplementary Fig. 1: D-OSKM reprogramming *in vitro* and *in vivo*.

- a**, A schematic illustration of the genomic construct for Dox-inducible LacZ ESCs.
- b**, Alkaline phosphatase staining for S-/D-OSKM MEFs after Dox treatment for 7, 14 and 21 days, followed by the withdrawal for 7 days. Scale bars: 10 mm.
- c**, Heatmap showing relative expression of MEF-related genes in S-/D-OSKM MEFs at Day 3. Repression of MEF-related genes were prominent in D-OSKM MEFs when compared with S-OSKM MEFs, indicating the rapid repression in D-OSKM MEFs. Color range is shown using a log₂ scale.
- d**, Gene ontology (GO) term enrichments of upregulated (left) and downregulated (right) genes in D-OSKM MEFs (Day 14) when compared with S-OSKM MEFs (Day 14) (Fold change>2, P<0.05). GO terms and the p-value are shown (Fisher's exact test, one-sided.). DAVID Bioinformatics Resources (v6.8) was used for the analysis.
- e**, Representative images showing mCherry signals in the kidney of S-/D-OSKM chimeric mice after Dox treatment for 10 days. Scale bars: 5 mm.
- f**, Flow cytometry analysis of kidney cells of S-/D-OSKM chimeric mice after Dox treatment for 7 days.
- g**, Un-supervised hierarchical clustering and PCA of transcriptomes of mCherry-positive *OSKM*-expressing kidney cells (Day 14).

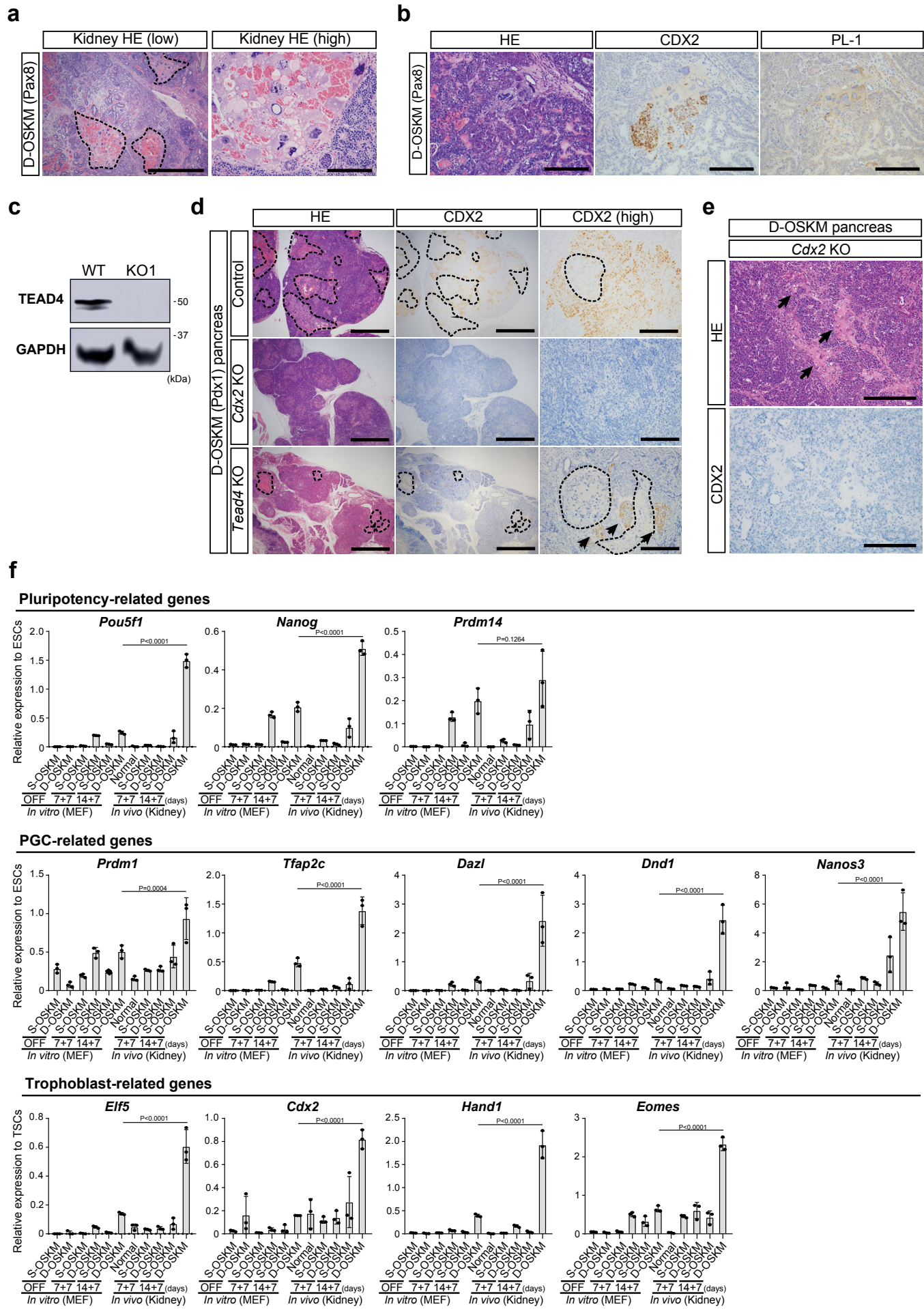
Supplementary Figure 2



Supplementary Fig. 2: Development of D-OSKM tumors that resemble human germ cell tumors.

- a**, Representative macroscopic images of pancreatic tumors in S-/D-OSKM chimeric mice. Scale bars: 5 mm.
- b**, Representative histological images and immunostaining for OCT4 and NANOG of S-/D-OSKM kidney tumors. Scale bars: 500 μ m.
- c**, Representative histological images of S-OSKM kidney and pancreatic tumors. Scale bars: 200 μ m.
- d**, Immunostaining for OCT4 of S-/D-OSKM kidney tumors. Scale bars: 200 μ m.
- e**, Quantification of the Ki67-positive cell ratio in the OCT4-positive cell area of S-/D-OSKM kidney tumors (n=10, respectively). The vast majority of OCT4-expressing D-OSKM tumor cells are positive for the cell proliferation marker Ki67, suggesting that the propagation of OCT4-expressing cells is responsible for tumor formation in the D-OSKM model. Data are presented as means \pm SD of biologically independent samples. (Mann–Whitney test, two-sided.)
- f**, Representative macroscopic and histological images of the D-OSKM kidney. Active cell proliferation in D-OSKM tumors was initiated after withdrawal of Dox, indicating that exogenous OSKM expression was dispensable for active proliferation of tumor cells. Immunostaining for 2A peptide and Ki-67 is shown in the right panels. Expression of 2A peptide represents exogenous reprogramming factor expression. Scale bars: 200 μ m.
- g**, Representative histological images of D-OSKM kidney tumors showing malignant features. Scale bars: 500 μ m (left and right), 200 μ m (middle).
- h**, Representative histological images and immunostaining for OCT4 of human embryonal carcinomas in the testis. Scale bars: 200 μ m.
- i**, Representative histological images and immunostaining for OCT4 and NANOG of secondary D-OSKM tumors in the subcutaneous tissue of immunocompromised mice. Scale bars: 200 μ m.
- j**, Representative macroscopic and histological images of D-OSKM tumors induced by low-dose Dox (kidney, 0.4 mg/mL; pancreas, 0.1 mg/mL). Scale bars: 5 mm (left), 500 μ m (middle and right).
- k**, Representative histological images of D-OSKM tumors (teratomas) induced by low-dose Dox. Scale bars: 200 μ m.
- l**, Representative histological images and immunostaining for OCT4 and DAZL of D-OSKM tumors. Scale bars: 500 μ m.
- m**, DNA methylation levels at genomic elements in D-OSKM pancreatic tumors measured by MethylC-seq analysis. CGI: CpG island; Non-CGI: Non-CpG island.
- n**, Total DNA methylation percentage in D-OSKM pancreatic tumors measured by WGBS.

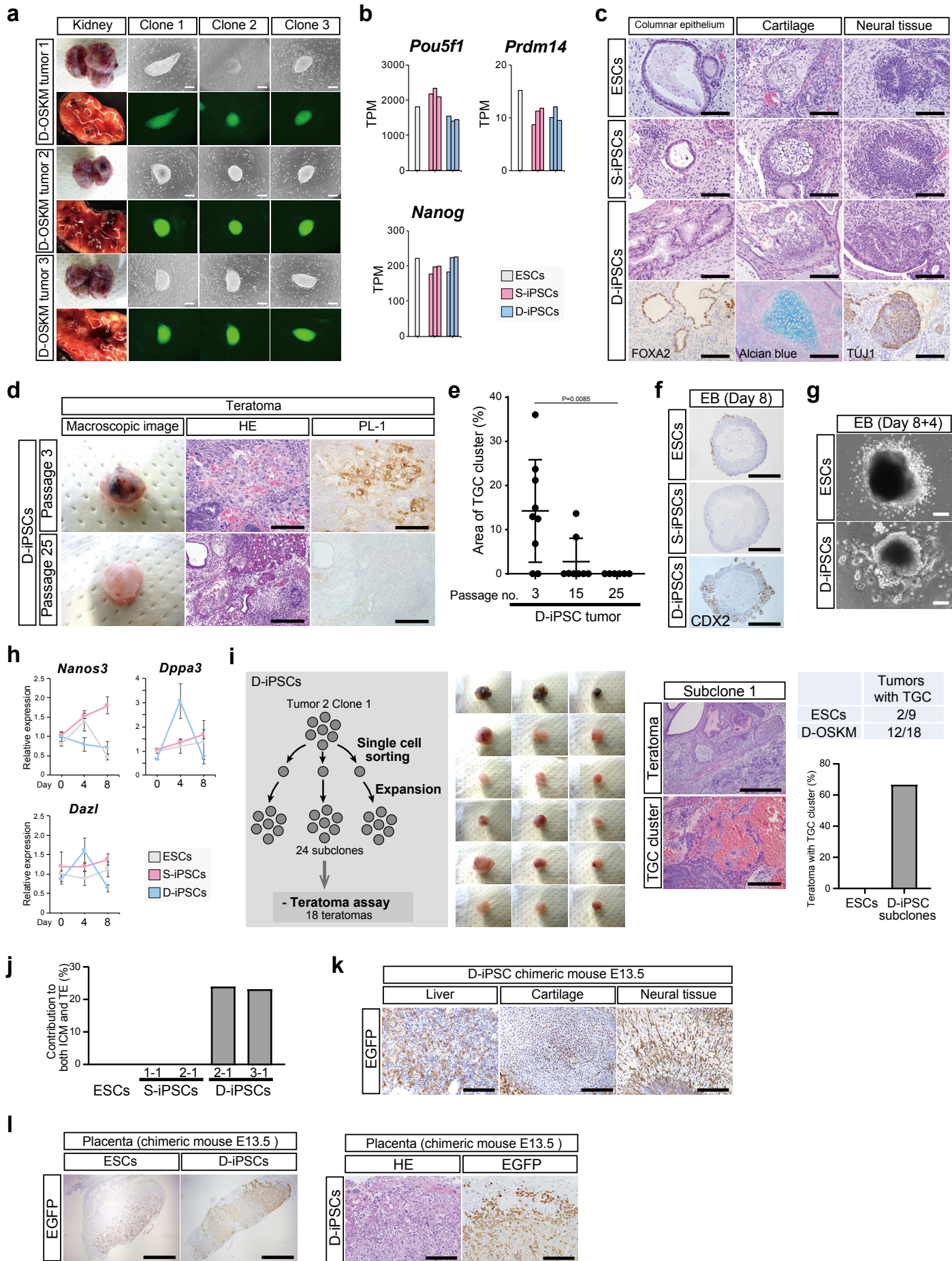
Supplementary Figure 3



Supplementary Fig. 3: Trophoblastic differentiation of D-OSKM tumor cells.

- a**, Representative histological images of D-OSKM kidney tumors with TGC clusters. Dotted lines indicate the TGC clusters. Scale bars: 500 μm (left), 200 μm (right).
- b**, Representative histological images and immunostaining for CDX2 and PL-1 of D-OSKM kidney tumors. Scale bars: 200 μm .
- c**, Western blotting for TEAD4 in *Tead4* KO D-OSKM ESCs. Lack of CDX2 protein expression was confirmed by immunostaining of D-OSKM tumors (see Extended Data Fig. 3d).
- d**, Representative histological images and immunostaining for CDX2 of D-OSKM pancreatic tumors. The number of trophoblast giant cells was significantly decreased in both *Tead4* KO and *Cdx2* KO D-OSKM tumors. A small population of trophoblast giant cells was still detectable in *Tead4* KO D-OSKM tumors, indicating the presence of an alternative trophoblastic differentiation pathway in D-OSKM tumors. Dotted lines indicate the TGC clusters, and arrows indicate CDX2-positive cells. Scale bars: 1000 μm (left and middle), 200 μm (left panels: right).
- e**, A small population of trophoblast giant cells was still detectable in *Cdx2* KO D-OSKM tumors, indicative of the presence of an alternative trophoblastic differentiation pathway. Arrows indicate TGCs. Scale bars: 200 μm .
- f**, qRT-PCR analyses for expression of pluripotency-, PGC- and trophoblast-related genes during reprogramming *in vitro* (MEFs) and *in vivo* (kidney). Data are presented as the means \pm SD of biological triplicates. Relative expression levels to ESCs are shown for pluripotency- and PGC-related genes. Relative expression levels to TSCs are shown for trophoblast-related genes. (one-way ANOVA and Dunnett's multiple comparisons test, two-sided.)

Supplementary Figure 4



Supplementary Fig. 4: Derivation of D-OSKM tumor-derived PSCs with differentiation potential toward extra-embryonic lineage.

a, Representative images of D-OSKM kidney tumors and iPSC-like cell colonies derived from D-OSKM kidney tumor cells. A total of nine D-iPSC clones were established from three independent kidney tumors. Scale bars: 200 μ m.

b, Expression levels of pluripotency-related genes in S-/D-iPSCs.

c, Representative histological images of subcutaneous tumors in immunocompromised mice. Scale bars: 200 μ m.

d, Representative macroscopic and histological images of subcutaneous tumors developed from D-iPSCs with different passage numbers (passage number 3 and 25). Immunostaining for PL-1 is shown in the right panels. Scale bars: 200 μ m.

e, Quantification of the TGC cluster area in D-iPSC tumors with different passage numbers (p3, n=9; p15, n=8; p25, n=6). Data are presented as means \pm SD of biologically independent samples. (Kruskal–Wallis test and Dunn’s multiple comparisons test, two-sided.)

f, CDX2 immunostaining of EBs at differentiation Day 8. Scale bars: 500 μ m.

g, Representative images of EBs after attachment on the gelatin-coated dish. Scale bars: 200 μ m.

h, qRT-PCR analyses for expression of PGC-related genes during EB formation. Data are presented as the means \pm SD of biological triplicates. The mean expression level of differentiation Day 0 ESCs was set to 1.

i, A schematic illustration of an experimental protocol for D-iPSC subclones. The majority of D-iPSC subclone-derived tumors contain clusters of TGCs. Scale bars: 500 μ m (upper), 200 μ m (lower).

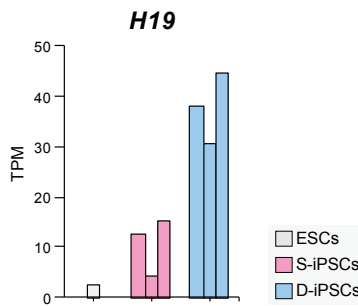
j, The frequency of blastocysts exhibiting GFP-labeled cells at both ICM and TE regions (ESCs, n=122; S-iPSCs 1-1, n=66; S-iPSCs 2-1, n=64; D-iPSCs 2-1, n=67; D-iPSCs 3-1, n=39).

k, GFP immunostaining of tissues in the E13.5 D-iPSC chimeric embryo. Scale bars: 200 μ m.

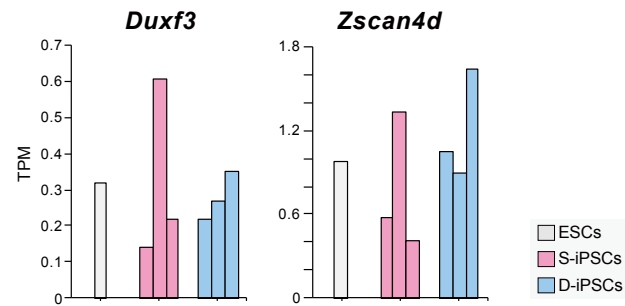
l, GFP immunostaining of the E13.5 chimeric placenta. Scale bars: 1000 μ m (left), 200 μ m (right).

Supplementary Figure 5

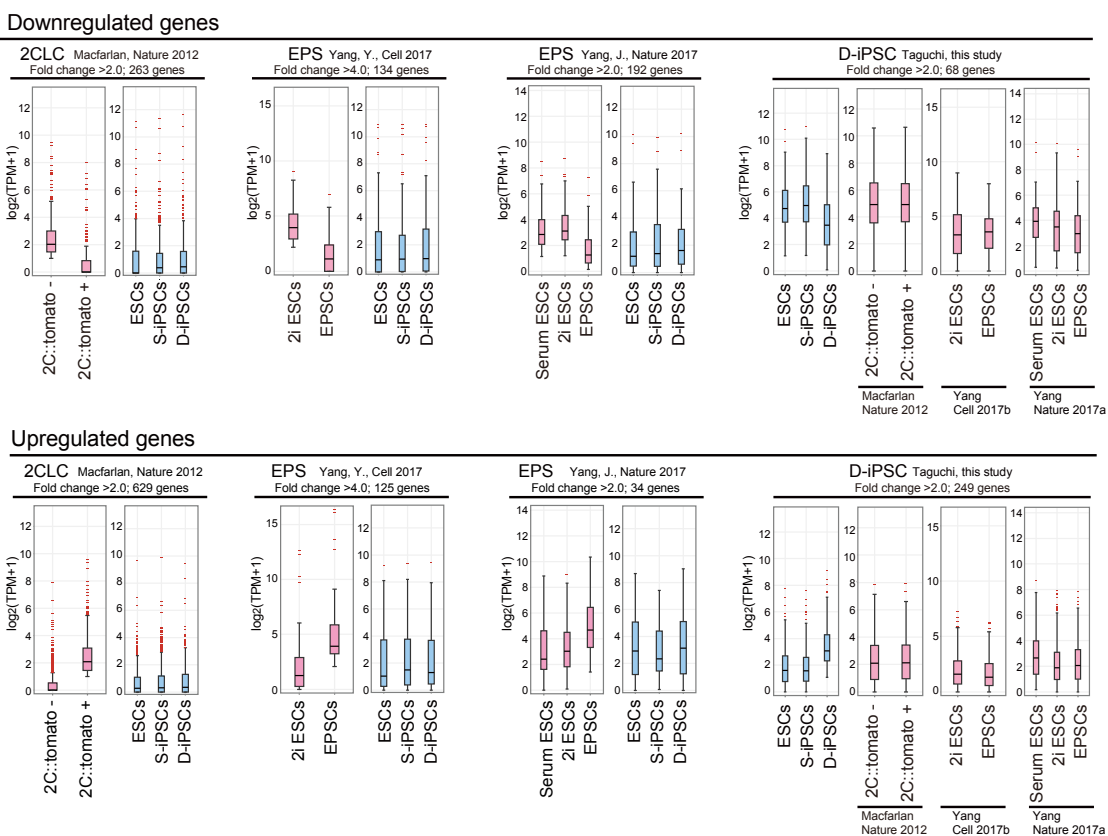
a



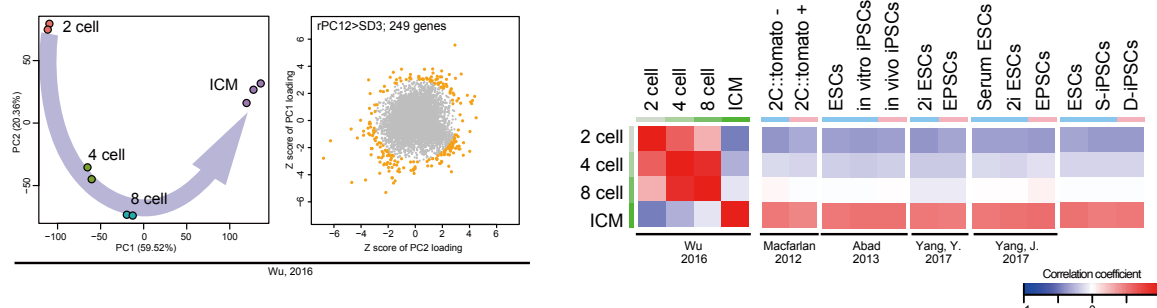
b



c



d



Supplementary Fig. 5: Gene expression profiles of D-iPSCs.

- a**, Expression levels of *H19* in ESCs, S-iPSCs, and D-iPSCs.
- b**, Expression levels of 2CLC-related genes in ESCs, S-iPSCs, and D-iPSCs.
- c**, Box plots for expression levels of upregulated/downregulated genes in each PSC type. Gene expression patterns of D-iPSCs were compared with previously reported mouse PSCs with expanded differentiation potential. Solid lines in each box indicate the median. The bottom and top of the boxes are lower and upper quartiles, respectively. Whiskers extend to ± 1.5 interquartile range (IQR). RNA-seq data of PSCs were obtained from GSE33923, GSE89303, and ERP005641.
- d**, PCA of the preimplantation embryos by all expressed genes (upper, left) from GSE66390¹. Scatter plot of the normalized loading scores of PCA (upper, right). Orange dots (249 genes) indicate genes that contributed highly to the PC1 and PC2 axes: >3 s.d. radius of PC1 and PC2 ($r_{PC12} > SD_3$)². Heatmap shows transcriptional correlation between preimplantation embryos and PSCs with expanded differentiation potential using the 249 genes from the upper panel³⁻⁶. RNA-seq data of PSCs were obtained from GSE33923, GSE48364, GSE89303, and ERP005641.

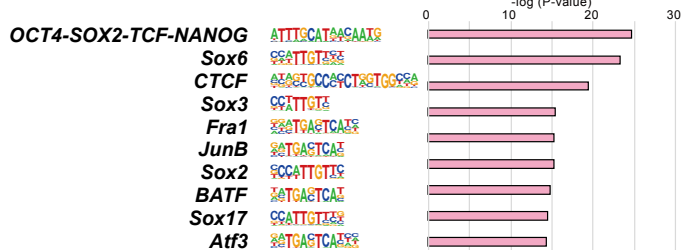
Supplementary Figure 6

a

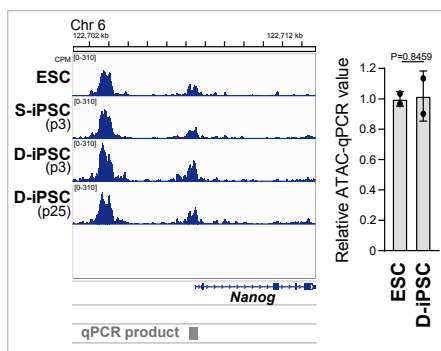
	Total read number	Mapping efficiency (%)
ESCs (LacZ)	125,787,010	96.7
S-iPSC (p3)	117,389,850	94.5
D-iPSC (p3)	116,012,340	96.4
D-iPSC (p25)	141,428,232	96.3

	Common peaks	Differential peaks		
		Enriched in D-iPSC (p3)	Depleted in D-iPSC (p3)	Overlapping peaks
vs ESCs (LacZ)	55,911	2,109	6,608	270
vs S-iPSC (p3)	56,078	1,860	6,623	
vs D-iPSC (p25)	55,458	1,787	3,773	
			Overlapping peaks 992	

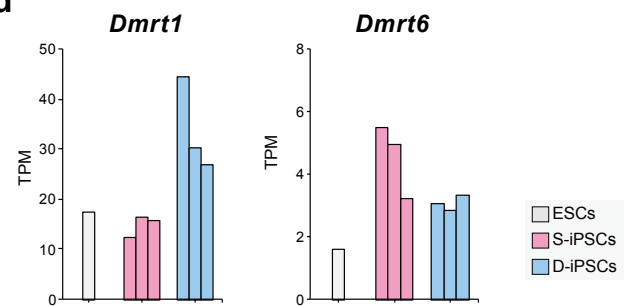
b



c



d



Supplementary Fig. 6: Elevated DMRT1 chromatin accessibility in D-PSCs.

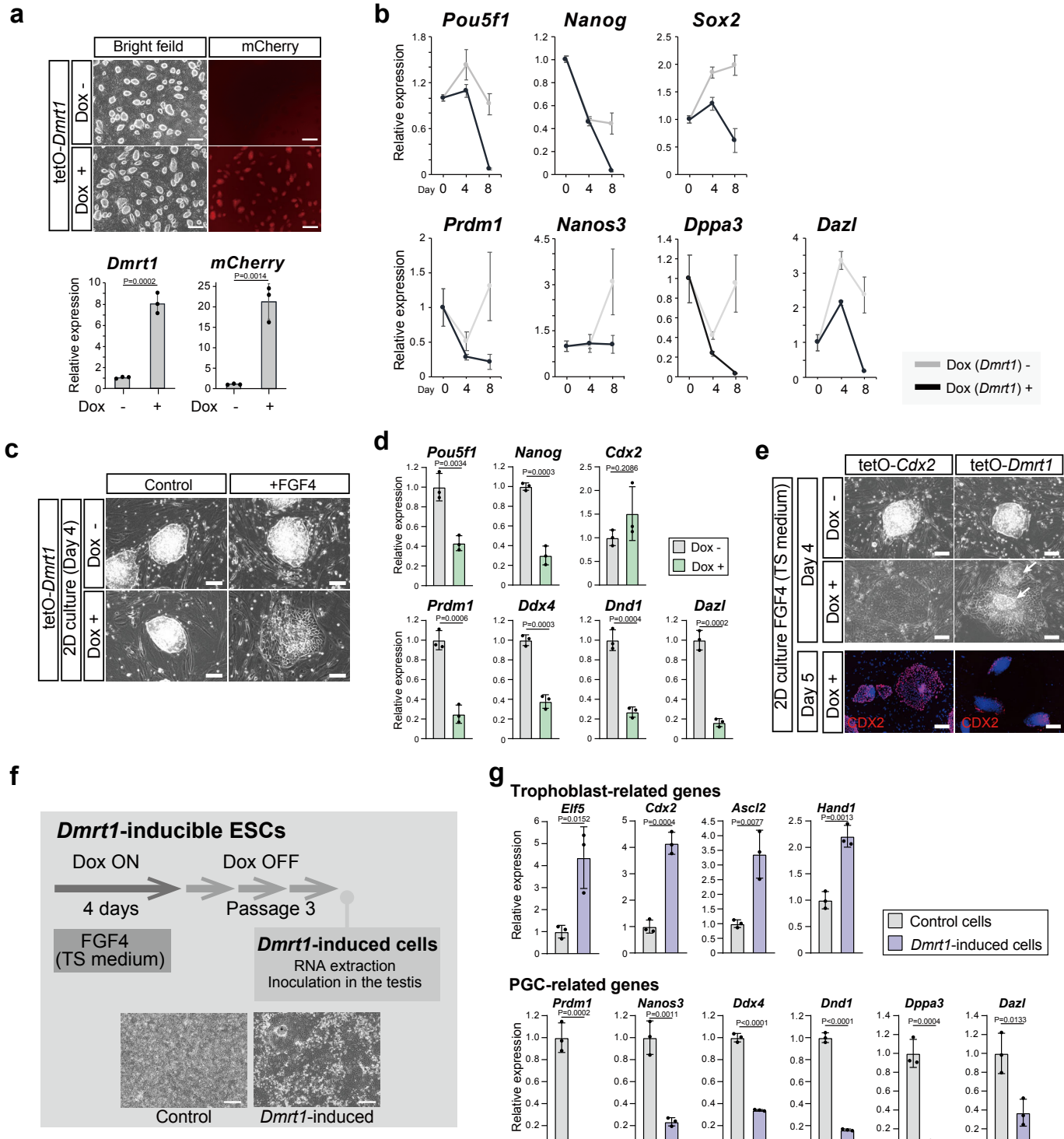
a, (Upper) Total numbers of ATAC-seq sequenced reads and the mapping efficiencies (ESCs, S-iPSCs (p3), D-iPSCs (p3) and D-iPSCs (p25), n=1, respectively). (Lower) Common and differential peaks in D-iPSCs (p3) that have bidirectional differentiation potential in comparison with other PSCs.

b, Motif enrichment analysis of D-iPSC-specific depleted peaks in ATAC-seq (n=992), performed using HOMER (Fisher's exact test, two-sided).

c, The *Nanog* locus was used for control peaks in ATAC-qPCR analysis. A genomic region of qPCR products is shown below. Data are presented as means \pm SD of biological duplicates. The mean ATAC-qPCR value of ESCs was defined as 1. (t-test, two-sided)

d, Expression levels of *Dmrt1* and *Dmrt6* in ESCs, S-iPSCs, and D-iPSCs.

Supplementary Figure 7



Supplementary Fig. 7: Elevated DMRT1 chromatin accessibility is associated with the expanded differentiation potential in PSCs.

a, Representative images and qRT-PCR analyses of Dox-inducible *Dmrt1* ESCs on Day 1 after Dox treatment. Scale bars: 500 μ m. Data are presented as means \pm SD of biological triplicates. Mean expression level of Dox (-) ESCs was defined as 1. (t-test, two-sided.)

b, qRT-PCR analyses of pluripotency- and PGC-related gene expression during EB differentiation of *Dmrt1*-inducible ESCs. Data are presented as means \pm SD of biological triplicates. The mean expression level of Dox (-) ESCs was defined as 1.

c, Representative images of *Dmrt1*-inducible ESCs treated in FGF4-containing culture medium. Scale bars: 100 μ m.

d, qRT-PCR analyses of pluripotency- and PGC-related gene expression in *Dmrt1*-inducible ESCs in FGF4-containing medium. Data are presented as means \pm SD of biological triplicates. The mean expression level of ESCs at Day 0 was defined as 1. (t-test, two-sided.)

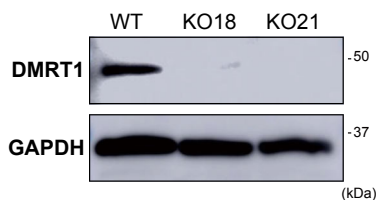
e, Representative images and CDX2 immunostaining of *Cdx2*- and *Dmrt1*-inducible ESCs in FGF4-containing medium (TS medium). Although *Cdx2* induction for 4 days caused rapid morphological changes in most ESCs, dome-shape colonies (arrows) were still present after *Dmrt1* induction for 4 days. Scale bars: 100 μ m (bright field), 200 μ m (CDX2).

f, Schematic illustration of the experimental protocol for transient induction of *Dmrt1*. Scale bars: 500 μ m.

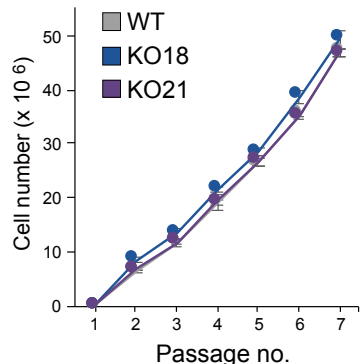
g, qRT-PCR analyses of trophoblast- and PGC-related gene expression in *Dmrt1*-induced cells. Data are presented as means \pm SD of biological triplicates. The mean expression level of control cells was defined as 1. (t-test, two-sided.)

Supplementary Figure 8

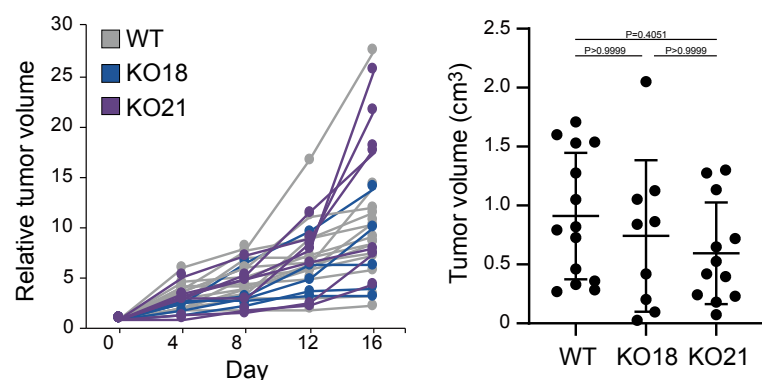
a



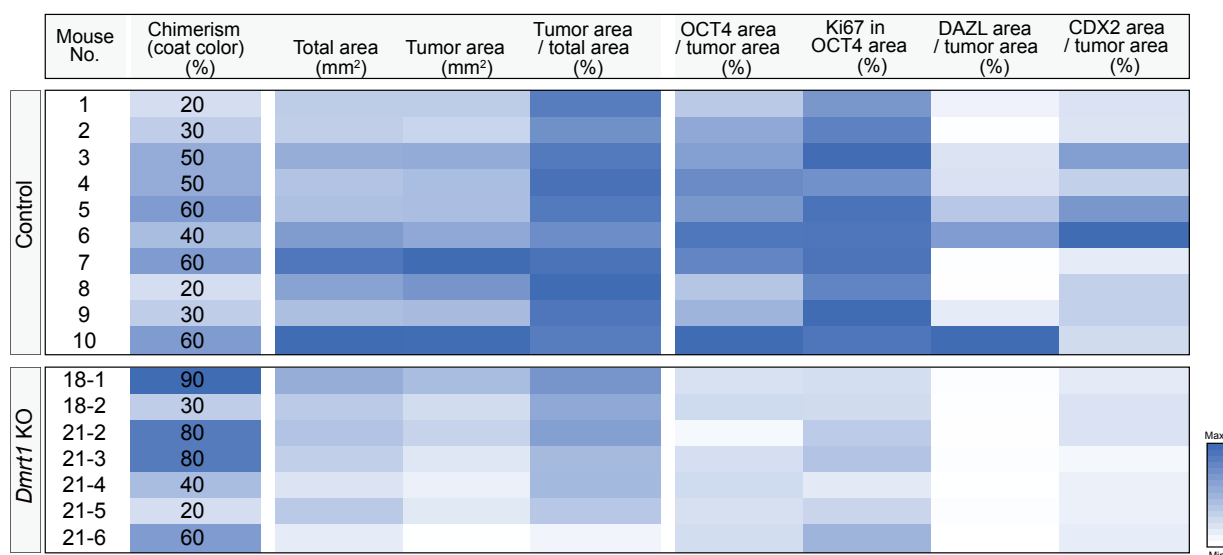
b



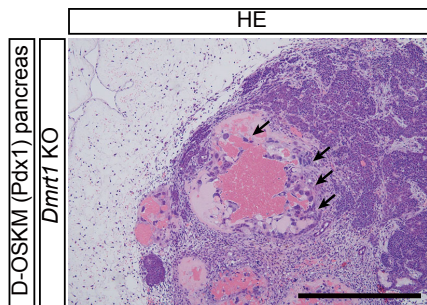
c



d



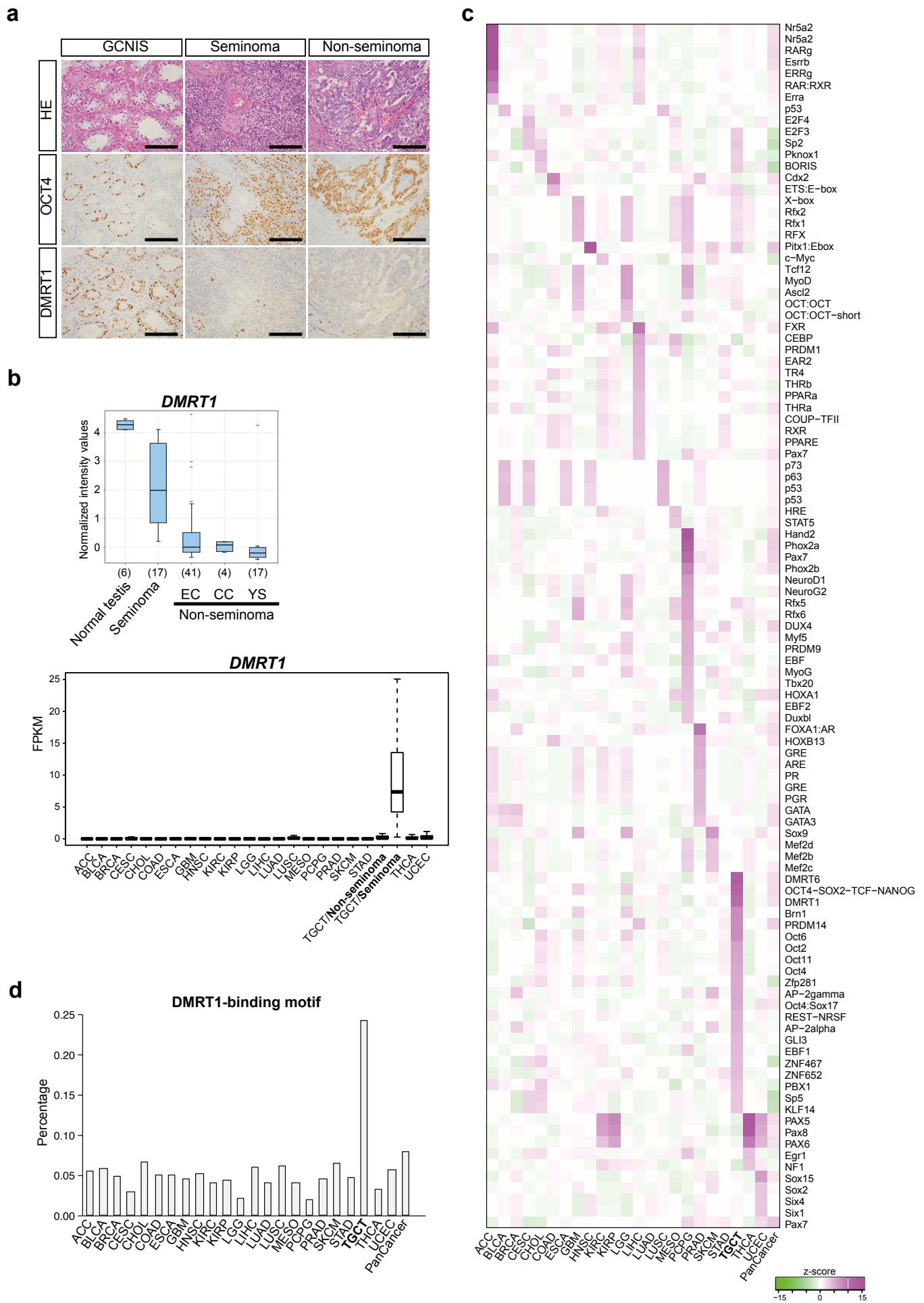
e



Supplementary Fig. 8: DMRT1 drives *in vivo* reprogramming and propagation of GCT-like tumor cells.

- a**, Western blotting for DMRT1 in *Dmrt1* KO D-OSKM ESCs.
- b**, Cell proliferation assay in *Dmrt1* KO D-OSKM ESCs. Data are presented as means ± SD of three independent experiments.
- c**, Tumor growth of *Dmrt1* KO D-OSKM ESCs in teratoma assay. Right panel represents tumor volume at Day 16 (control, n=14; *Dmrt1* KO ESCs [KO18, n=8; KO21, n=12]). Data are presented as means ± SD of biologically independent samples. (t-test with Welch's correction, two-sided.)
- d**, Coat color chimerism in each *Dmrt1* KO chimeric mouse used in this study. Quantification of histological analysis is summarized for each mouse that developed pancreatic tumors.
- e**, Histological image of *Dmrt1* KO D-OSKM pancreatic tumor. Although *Dmrt1* KO D-OSKM tumors exhibited a significant reduction in CDX2-positive cells, D-OSKM tumors still contained clusters of trophoblast giant cells (arrows), suggesting the presence of an alternative pathway for differentiation into trophoblast giant cells. Scale bars: 500 μm.

Supplementary Figure 9



Supplementary Fig. 9: DMRT1-mediated reprogramming in human germ cell tumors.

a, Representative histological images and immunostaining for OCT4 and DMRT1 in human testicular neoplasms (GCNIS: Germ cell neoplasia in situ). Note that GCNIS exhibits the highest expression of DMRT1. Scale bars: 200 μ m.

b, (Upper) Box plot showing expression of *DMRT1* in human testicular GCTs (normal testis, n=6; seminoma, n=17; non-seminoma [EC: embryonal carcinoma, n=41; CC: choriocarcinoma, n=4; YS: yolk sac tumor, n=17]). Microarray data were obtained from GSE3218⁷. Solid lines in each box indicate the median. The bottom and top of the boxes are lower and upper quartiles, respectively. Whiskers extend to ± 1.5 interquartile range (IQR).

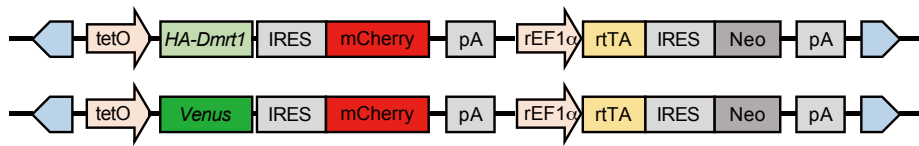
(Lower) Box plot showing FPKM (expression levels) of DMRT1 in 23 types of human cancer. Solid lines in each box indicate medians. The bottom and top of the boxes indicate the lower and upper quartiles, respectively. Whiskers extend to ± 1.5 interquartile range (IQR). Each cancer type expression dataset, obtained by RNA-seq, was obtained from the NIH GDC Data Portal (<https://portal.gdc.cancer.gov/>).

c, Heatmaps are shown as in Fig. 7b. Transcription factors are ordered based on the proportions of cancer type-specific open chromatin regions with their consensus motifs. The dataset from Fig. 7b was used.

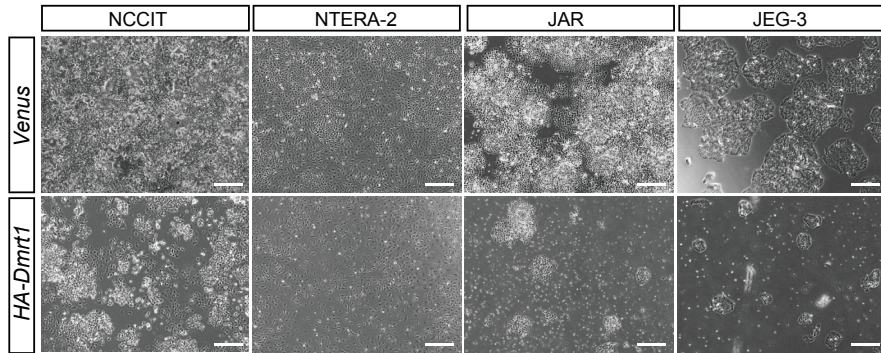
d, Proportion of each cancer type-specific open chromatin region that contains DMRT1 consensus motifs. The dataset from Fig. 7b was used.

Supplementary Figure 10

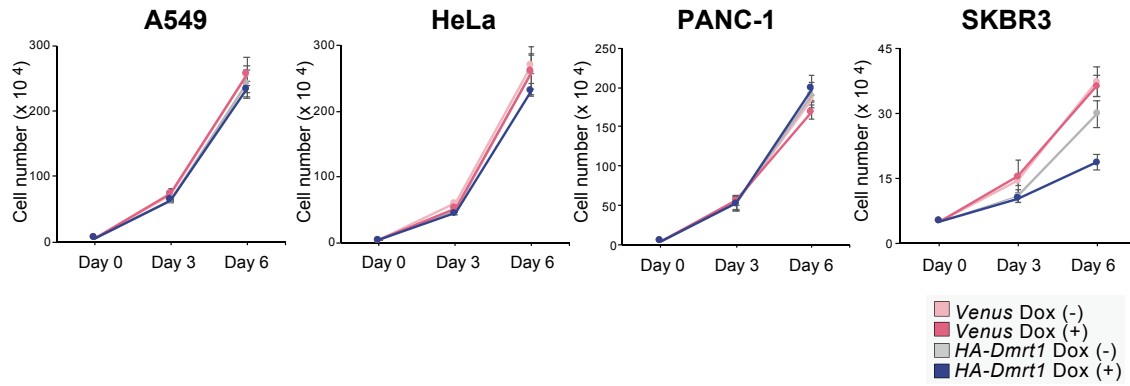
a



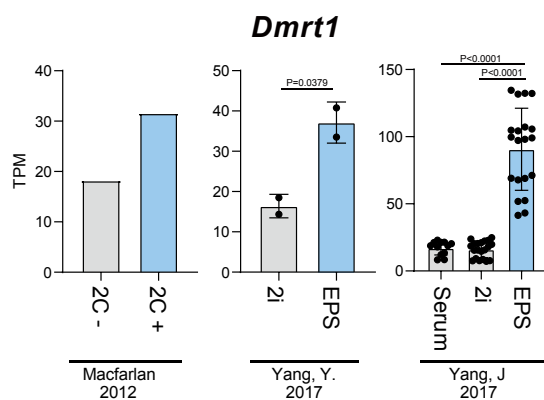
b



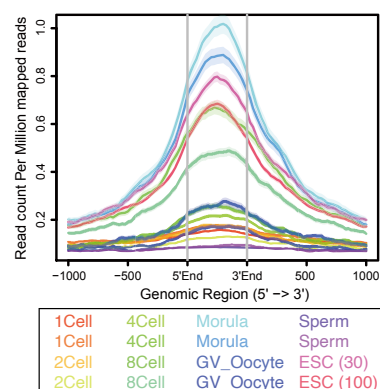
c



d



e



Supplementary Fig. 10: DMRT1-mediated reprogramming provides a unique therapeutic target for human germ cell tumors.

- a**, Schematic illustration of the *piggyBac* vector construct for Dox-inducible *Dmrt1* or *Venus*.
- b**, Representative images of human GCT cell lines carrying Dox-inducible *Dmrt1* or *Venus* alleles after Dox treatment (NCCIT, Day 5; NTERA-2, Day 6; JAR, Day 6; JEG-3, Day 6). Scale bars: 500 μ m.
- c**, Cell proliferation assay in *Dmrt1*-expressing human cancer cell lines (A549: lung adenocarcinoma; HeLa: cervix epithelioid carcinoma; PANC-1: pancreas ductal adenocarcinoma; SKBR3: breast adenocarcinoma). Data are presented as means \pm SD of three independent experiments.
- d**, Expression levels of *Dmrt1* in previously reported mouse PSCs with expanded differentiation potential. RNA-seq data of PSCs were obtained from GSE33923 (2C::tomato-, n=1; 2C::tomato+, n=1), GSE89303 (2i, n=2, EPS, n=2) and ERP005641 (Serum, n=12; 2i, n=20; EPS, n=20). Data are presented as means \pm SD (Yang, Y., 2017⁶: t-test, two-sided; Yang, J., 2017⁵: Kruskal–Wallis test and Dunn’s multiple comparisons test, two-sided.).
- e**, DNase-seq analysis for DMRT1 binding sites in E13.5 gonadal cells in preimplantation embryos at various developmental stages. The DMRT1 binding sites were the most accessible at the morula stage during preimplantation embryogenesis. Shading represents the standard error of the mean (SEM).

Reference

1. Wu, J.Y. *et al.* The landscape of accessible chromatin in mammalian preimplantation embryos. *Nature* **534**, 652-+ (2016).
2. Nakamura, T. *et al.* A developmental coordinate of pluripotency among mice, monkeys and humans. *Nature* **537**, 57-62 (2016).
3. Abad, M. *et al.* Reprogramming in vivo produces teratomas and iPS cells with totipotency features. *Nature* **502**, 340-5 (2013).
4. Macfarlan, T.S. *et al.* Embryonic stem cell potency fluctuates with endogenous retrovirus activity. *Nature* **487**, 57-+ (2012).
5. Yang, J. *et al.* Establishment of mouse expanded potential stem cells. *Nature* **550**, 393-397 (2017).
6. Yang, Y. *et al.* Derivation of Pluripotent Stem Cells with In Vivo Embryonic and Extraembryonic Potency. *Cell* **169**, 243-257 (2017).
7. Korkola, J.E. *et al.* Down-regulation of stem cell genes, including those in a 200-kb gene cluster at 12p13.31, is associated with in vivo differentiation of human male germ cell tumors. *Cancer Research* **66**, 820-827 (2006).

Table S1. Primer used in this study.

qPCR		Sequences (5'→3')	
	Forward	Reverse	
Mouse: Actb	GCCAACCGTGAAGAGATGAC	TCCGGAGTCATCACAATG	
Mouse: Pou5f1	TAGGTGAGGCCCTTTCAC	GCTTAGCCAGTTGGAGAT	
Mouse: Sox2	CGTAAGATGGCCAGGAGAA	GCTTCGGCTCGGACAAA	
Mouse: Klf4	GACTAACCGTGGCTGAGGA	CTGCAAGTCACAGCCTC	
Mouse: Myc	CACCAAGCAGGACTCTGA	GGGGTTTGCTCTTCTCC	
Mouse: Nanog3	CACTACGGCTAGGAGCTGG	TGATGGCTGACAAGACTGG	
Mouse: Dazl	TCTTGTAGCTGTGTCG	CCACCTCGAGGTTTACCA	
Mouse: Dppa3	AGGCTCGAAGGAAATGAGTTG	TCTTAATCTTCCGATTITCG	
Mouse: Dmrt1	GAAGACCTAGAGAGCCGC	CCTTCCTGAAGGAAAGATCTGGG	
Mouse: mCherry	CCCGCCGACATCCCGACTA	GGGTCAGGTCACACGCC	
Mouse: Dbx4	TATGTTGCCCTCCAGCTTCA	CTGGATTGGAGCTTGAAAGA	
Mouse: Nanog	TGCTTACAAAGGTCTGCTACTG	TAGAAGATAAGGGCTGCC	
Mouse: Prdm14	ACAGCCAAGCAATTGCACTAC	TTACCTGGCATTTCTATGTC	
Mouse: Dnd1	CCCTAAATGGGTTAACAGAGC	GCGAAGGTTCTCACAACAAAG	
Mouse: Cdx2	CAAGGACGTGAGCATGATC	GTAACACCGTAGTCGGGTA	
Mouse: Prdm1	GCCACAAGAGATTTAGCAGCACAA	CAGTCGCTGTGAGCTTCAG	
Mouse: Hand1	GCTCCACGAACCCCTCTG	CAGCAGCAGCTCTGGAAAGTA	
Mouse: Ascl2	GAGCAGGAGCTGCTGACTT	CAGTCAGCACTTGGCATTTG	
Mouse: Elavl	GACCAAGCCATGTCG	CAGGCCGCTAGTGTGAAGTG	
Mouse: Eomes	GATGTACGTTACCCAGAACATCTCT	CATCTGTTGTTGTTGTTGAC	
Mouse: Timp2c	GGCACACATCTCATGTCGGG	CGAGATGTCAGCTGCTGTA	
Human: GAPDH	ATGGGAAAGGTGAAGGTG	GGGGTCATTGATGCCAACATA	
Human: GATA3	TGCAGGAGCAGTATCATGAAGCT	GCATCAAACACTGTGGCAGTGA	
Human: GATA2	GCACCTGTTGCAAATTGAGA	CTGGATCCCTCTCTCATG	
Human: KRT7	GGCTGAGTACCAAGGAACATCATG	GCTTGGGTAGGTGGCG	
Human: HLA-G	GCTGTGATCACTGGAGCTG	ACTCTGGCTCTCAGTCCC	
Human: CGB	CAACACCAACTGTC	CTTATGTTGGGAGGATC	
Human: p16 (INK4A)	GTGCCACATTCGTAAGTGCTC	CGACCCGTCTCCAAATCTC	
Human: p15 (INK4B)	GTCATGATGATGGGAGCGC	CAGCATCATGCAACGGTGC	
Human: p18 (INK4C)	GATTGGAAGGACTGGCTGC	CATGAATGACAGGAAACCGATCG	
Human: p19 (INK4D)	GCTTCTGGCAGCTGAATCTGATC	CTCTGCTGGAGGGTGACC	
Human: p21 (CIP1)	GACCATGTTGACCTGCACTGT	CCGTTTTCGACCTGAGAGTC	
Human: p27 (KIP1)	GAGCAATGCGAGGAATAAGGAA	CTCCACAGAACCGGATTGG	
Human: p57 (KIP2)	GGGGCGATCAAGAAGCTGC	CTGCTCACCGGAGGCCA	
Bisulfite sequencing		Sequences (5'→3')	
	Forward	Reverse	
H19 DMR (Outside)	GAGTATTAGGAGGTATAAGAATT	ATCAAAAACATAAAACCCCT	
H19 DMR (Inside)	GTAAGGAGATTATTTGTTTTTGG	CCTCAITAATCCCTAAACTAT	
Nespa-Gnax1 DMR	GGTITGGGTTTGTGTTGTTATTTA	TCCTCTAAAATCCACTAAATCTCACTACC	
Cloning		Sequences (5'→3')	
	Forward	Reverse	
Cre-pA-PGK-Bsd-pA (Pax8)	GTAGGAAAGCTGGAGTGTCTCTAGCTGTGAGCAGCTCCGGGATGCCAAGAAGAAGAGGAAGGT	GGGGTCTGGCCCTCCGGCTCTACGGATCTGATCGAGTTGAGGCTAACCTTAAATGCCAATTATTTAAAGTTAT	
Cre-pA-PGK-Bsd-pA (Pdx1)	GCTCTGTCCTCGACCCGGGGCTGCTGGCCCCAAGTGGCGCTGCCACCATGCCAAGAAGAGGAGGTG	CACGGTCTCTTGTAGACTGCTGTCGGCGCTAGTAGCTGCTCTACTGTTCAACTTTAAATGCCAATTATTTAAAGTTATGAACTCAGACATG	
Osf4-P2A-Sox2-T2A-Klf4-E2A-e-Myc with Kozak sequence	GCCACCATGGTGGACACCTGGCTTC	TTATGCACCATGGTGGACAGCTG	
Venus with Kozak sequence	GCCACCATGGTGGACAGGGGAGGG	TTACTGTACAGCTGTCATGCC	
P2A-CreERT2-pA-PGK-Bsd-pA (Nanog)	AAGCTTGGAAATTATTCGAACTACTCTGACTCCACCCAGGTAAATAGCAGCGCAGCG	AGGAACCTGGCTTGGCTACTTAAAGCCAGATGTGCTAAGCTCAAGACATGATAAGATAACATTGATGAGTTGGACA	
HA-Dmrt1	ATGTACCCCTACGGCTGGGACTACGCCGGAACGACGACATCG	TCACTGCTCTCATCTCTTCC	
Dmrt1 with Kozak sequence	GGCACCATGGCAGCACACATT	TCACTGCTCTCATCTCTTCC	
HA-Cdx2	ATGTACCCCTACGGCTGGCCTACGCCCTACGTGAGCTACCTCTGGACAAG	TCACTGGGTGACAGTGGAGTT	
Knockout experiments		Sequences (5'→3')	
	Forward	Reverse	
Cdx2	GTTTGCCCCAGACAGCATGG	CATCCACTCGCACAGGTTTCG	
Tead4	GTITATACCCCTGGTCCCCA	CCAGGTGCGCTGGCAAG	
Dmrt1	GTACAACCCCAACCCACT	CTGCACTCTGCACTGGCA	
ATAC-qPCR		Sequences (5'→3')	
	Forward	Reverse	
Rpl12	ACCTCTGGTGCAGCCCTAC	GAGCTTGGCTGTGGTGAG	
Chr11	ACAGGAAAAACTCAAAGCTAC	TCCTTCCCCAGCTTGAGTT	
Chr4	CATGCCGTAATGCTAGCAC	AGGATGCTCTGCGCTGCTA	
Nanog	GGCAGCAAGCTGACTCTT	CTTTAACACCGCTGCA	